Research Article

High energy laser & systems to neutralise stellar coronal mass ejections (CME) plasma

Abstract

With CME plasma and shockwave travelling at 600+ km/sec, active methods such as high energy electron lasers (HEL) and mirrors are effective at making contact with ionised atoms in CME. Electrons pulsed from kW to MW laser(s) could polarise ionised atoms such as $Fe16+$, $O7/8+$, Mg, $He2+$,etc to fill valence pairs. As high-FIP atoms are electromagnetically trapped with a higher susceptibility from lower e- density and temperatures, CME plasma clouds can be neutralised, separated, and reduced in velocity trajectory around planet.

Study outlines interactions between Electron Laser and CME plasma cloud, orbital geometry, build of high energy lasers, subsystems, as well as recoils, and cloud charge dynamics with e- interactions to neutralise CME particles. Additional space-based systems are designed such as mirrors in closer orbit to align lower velocity light beams. In approaching higher electron recombination and FIP ionisation of laser-plasma ion cluster density, max absorption of e- to CME could be approached with similar beam, CME, mirror angles and alignment, where e- couple and fill valence shells.

Models evaluate efficacy of coherent laser beams of charged electrons, X-rays, infrared (IR), and/or electron/radio Hz to polarize CME column charge densities, with optimal CME scatter geometry and time window. Low cost ground experiments are discussed. Models suggest every ~1 km gap laser creates when CME t=8.255min creates a 10,067 km gap for Earth to orbit through. Such a HEL laser, reflecting mirrors, and space systems could neutralize plasma CME Cloud within 92.818M mi (Sun-Earth distance) and mitigate effects and trillion dollar costs from Carrington-type CME flares, and supernovae.

Keywords: space systems, coronal mass ejection, high energy laser, astrophysics

Kolemann Lutz,[1] Terry Trevino[2]
[1]University of Virginia, Magneto Space, USA
[2]University of North Dakota, Magneto Space, USA

Correspondence: Kole Lutz, University of Virginia, Magneto Space, Washington DC, USA, Tel +17032448456, Email pxr2v@virginia.edu

Abbreviations: AU, astronomical units; BLP, beam laser propulsion; CME, coronal mass ejection; CPA, chirped pulse amplification; EMC, electromagnetic compatibility; FIP, first ionisation potential; FEL, free electron laser; HEL, high energy lasers; IC, intracloud lightning; IFEL, inverse free electron laser; ICS, inverse compton scattering; LPA, laser-plasma accelerator; LPP, Laser Pulse Parameters; LOS, line of sight; MHD, magnetohydrodynamics; SASE, self-amplified spontaneous emission; SEP, solar energetic particle events; VEDs, viscoelastic dampers.

Key takeaways

i. Early models suggest potential to achieve CME free Earth safe zone gap and additional hours-day to impact from laser buffer time, which could reduce radiation flux experienced on planet.

ii. A CME Clearance Arc Length Ratio of 1 $CME_{t=8.255}$: 10,067km $CME_{t=1AU}$ suggests for every ~1 km gap laser creates when CME t=8.255min creates a 10,067 km gap for Earth to orbit through.

iii. To neutralise ions when CME at t=8.255min to provide $CME_{Clearance Arc Length}$ of 4.29km for Earth to orbit through, laser or electrons would neutralise 789.98 (km^2/min) for $d_{Earth-Safe-Zone}$ 43,164km gap around GEO.

iv. Reflecting Mirrors in close orbit such as Mercury are discussed to align electrons and CME in phase for recombination and pairing in plasma cluster layers with potential to recover 50-90%+ of beamed energy.

v. If approaching $\theta_{Laser} \approx \theta_{CME} \approx \theta_{Mirrors}$ yields greater electron-CME recombination rates, this suggests mirror architecture and greater rates of EMC and e- pair fill rates/degree to neutralise charged ions such as Fe^{16+}.

Introduction

The frequency of collisions of compact CMEs with the young Sun is ~0.3 events day to 1 CME event per day.[1] The frequency of Carrington-type flares (2×10^{32} erg) are about 200 events per year or about one event per day with severe space super-storms occurring every 42 of 150 years. In 1859, a CME of 3-4 X 10^32 ergs impacted Earth and electrical infrastructure to be known as Carrington event. In 2013, insurance firm Lloyd's of London calculated that in the case of another Carrington type event, the outage could cost up to $2.6 trillion and US alone at US$600 billion. With impacts, primarily on human activities in space, with today's modern electromagnetic infrastructure on ground and 7,700+ active satellites in 2023 in orbit, high energy ionised particles from CME plasma would create charged material defects in semi conductors and bit flips in electronic materials (Figure 1).

Spikes of carbon-14 seen in the years 660 B.C., A.D. 774 and A.D. 994 may have come from superflares that were significantly stronger than the Carrington Event. While superflares ~10X more energetic than the Carrington Event happen every ~3,000 years. Moreover, multiple supernovae released Neutrinos or fermions, i.e. elementary particles such as electrons with a spin of ½, at distances of ~100 pc consisting of two main events: one 2.59M years ago at end of Pliocene epoch, and the other at 6.5 to 8.7 million years ago. Tropospheric ionisation penetration of ≥TeV gamma, cosmic, Xrays would be increased by an order of magnitude for thousands of years, increasing radiation by 20-fold and triple radiation load on terrestrial organisms.
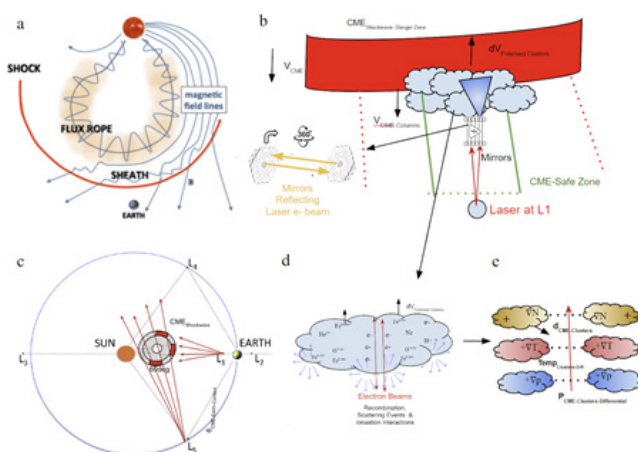
Figure 1 a) CME and shockwave, b) Interactions between CME plasma clusters, electromagnetic mirrors, c) Orbital geometry of electron laser at Earth-Sun L1, mirrors in mercury orbit, and d) CME plasma-laser cloud element gradient interactions.

CME observations, composition, data

The Sun's mass is 73% hydrogen, ~25% is helium, and .2% C, .8% atomic oxygen, .16% Ne. Various metals make up less than 0.1% of the mass of the sun. CMEs have masses of 10^{15}-10^{16}g with radial size of 0.25 astronomical unit (AU; 37 million km, or 23 million miles) when reaching Earth at 1 AU (150 million km). Two main types of CMEs are cool and hot as most CMEs discussed refer to the hot type. CMEs are accelerated in the corona compared to flare events and are faster. With CME's erupting from active stronger stars at average speed of 489-600 km/sec @ 20nT (at L1 at .15AU), CME speeds correspond to transit times to Earth's orbit of 13 hours to 86 days (extremes), with 2-3.5 days average.[2] Accelerated by magnetic field of CME plasmoid pushing against the surrounding magnetic field.[3] CMEs have increased EM field strength, smooth rotation of the magnetic field vector, and low proton temperature.[4] With electromagnetic flux rope trapped in stellar EM fields, kink instability results in rope unstable to further twisting, & torus instability results in rope unstable to further expansion.

Particles in flare EM electromagnetic clouds include bidirectional superthermal abundance of iron, helium, carbon, and/or oxygen electrons with more polarised charge states. CME elemental composition data for Fe, Mg, Si, S, C, N, Ne, O, and He is outlined from found that ion distributions in an ICME can be remodeled from ions generated within four distinct plasma components (PCs) with thermodynamic histories for C,O, and Fe. In solar wind, charge states of heavy ions can freeze in at heights when expansion timescale is equal to recombination timescale at 1–5 solar radii.[5,6] Three parameters: freeze-in temperature, relative abundance, and kappa value (κ) together describe potential non-Maxwellian kappa distributions of coronal electrons.[7]

Ionisation and electron recombination rates are functions of the electron density.[8,9] Using the CHIANTI database, electron distribution in the corona may be in ionization equilibrium prior to acceleration.[10] Developed a model on ion charge states in halo CMEs. CMEs exhibit an abundance increase of elements with first ionisation potential (FIP) < 10 eV, as well as a significant increase of Neon as compared to quasi-stationary solar wind. When the Fe ionic charge states are elevated above QFe > 12.0, FIP is greatest. In a Study of Coronal Features Associated with 57 CMEs on Sun, 43 (or 75%) of them exhibited at least 6 consecutive hours of QFe > 12.0. Fe charge

states >16+ are often observed in the presence of CMEs at 1 AU. Researchers analyzed averaged charge-state distributions of iron ions of 310 ICMEs from 1998 to 2011 with detailed composition of iron ions based on multipopulation from.[7] Simulations of Solar Energetic Particle (SEP) Fe and O propagation within a Parker spiral magnetic field in the presence of weak rigidity-independent scattering found that significant drift is experienced by Fe and O ions away from the flux tube in which they were initially injected.[11] Further data is outlined in Supporting Information attached document.

Elevated charge states are reflection of FIP elements stem from initial conditions from material in active region corona before plasma ejection. Models and measurements observed increases in both O7+/ O8+, Above 106 K, O would be mainly O8 +, instead of O7 + and O6 +. Fe behaves similar to Ne and Argon-like charge state Fe16+or above, which have small recombination rates. Elements with FIP larger than 10 eV are less abundant relative to O at ~80% and He at 50%.For CMEs with elevated charge states, the FIP effect is enhanced by 70% compared to slow wind.[12] Which suggests + and/or - polarity of plasma could play a role in CME scattering and deflection. For the Fe ionisation balance, CMEs have peaks around Fe16+ and Fe8+ (the Ne-like and Ar-like charge states, and more research may quantify electron recombination rates.

Magnetic stellar field lines are critical to determine deflection and rotation of stellar CMEs. In Figure 2 B, e- are accelerated and flow out into both post-flare loop and into the erupting prominence and related magnetic flux rope prior to clustering and recombination in CME Plasma columns and clusters. Recent magnetohydrodynamnic (MHD) simulations of stellar compact CMEs initiated from active regions are outlined from Alvarado-Gomez et al.,[13] 3D Model FOreCAT can be utilised to model anisotropic CME trajectory and frequencies. (Kay, et al, 2019) 3D MHD simulations, inversion of VL polarised data allows to determine CME speed and 3D propagation direction (with the polarisation ratio technique), as well to derive information on extension along the LOS of the emitting plasma, which is a crucial parameter to convert plasma electron column densities and temp.[14]
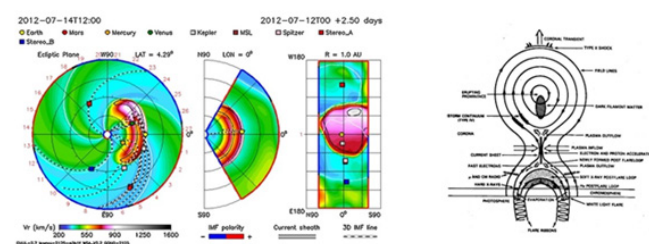

Figure 2 a) CME Solar wind radial velocity contour plots (Gil, et al, 2020) and b) CME diagram with two ribbon flare model with energy conversion processes (adapted from Martens and Kuin,1989).

With rapid acceleration within several tens of minutes, CME's accelerate from 200 to 2,000 km/sec from shockwaves manifesting as electromagnetic clouds with plasma reaching 1 MK that can stretch 1.6 million km's long. CMEs sweep up charged particles from the solar wind. The radial velocity of the CME eject varied from over 600 km s−1 at the leading edge to about 500 km s−1 at the core, suggesting an expansion.[15,16] Comparison of CME radial velocities from a flux rope model with correlations (R>0.9).[17]

Photoelectric effect, compton scattering, and absorption

Compton Effect is in between Coherent Scattering and the photoelectric effect. The X-ray comes in, it's scattered and an electron

is scattered as well as electron deposits its energy locally. The likelihood of such interactions with inner shells depends strongly on atomic number Z (i.e. Z3). When electrons are absorbed and move to inner energy levels, they conserve energy and emit secondary X-ray photons. Non-linear inverse Compton scattering (NICS) is the scattering of multiple low-energy photons, by a high electromagnetic field such as from a laser (Figure 3).
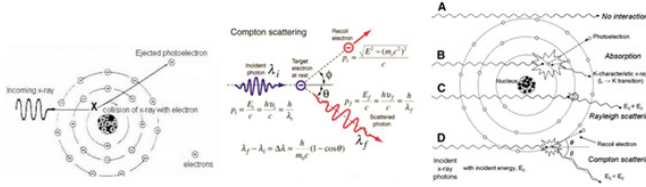

Figure 3 Non-linear inverse Compton scattering (CICS), with mathematical analysis of the photoelectric effect is outlined from (Bach, 2001), b) Absorption vs scattering.

Free electron lasers (FEL), design, engineering, materials

Free Electron Lasers FEL pass electrons through a magnetic structure known as an undulator or wiggler that aligns electron phase and spin through alternating EM fields to create coherent dense laser. Beam passes through magnets with alternating poles across the beam path, creating an alternating EM field. One of the greater benefits of Free-electron lasers is that they are tunable from changing electron energy to accommodate for a wider frequency range than any other type of laser (F. J. Duarte (Ed.) (Figure 4).
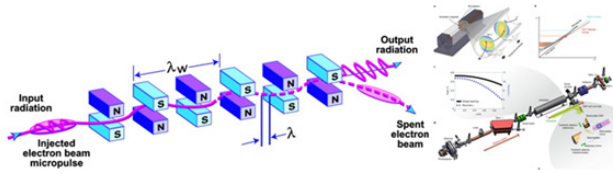

Figure 4 Pegasus beamline drawing with THz diagnostics and zero-slippage FEL interaction between relativistic electrons (Fisher, et al, 2022).

To design a high-efficiency terahertz free-electron laser, researchers used a circular waveguide in a 0.96-m strongly tapered helical undulator to match the radiation and electron-beam velocities, allowing resonant energy extraction from an ultra short 200-pC 5.5-MeV electron beam over an extended distance. Average energy efficiency of 10% with some particles losing >20% of their initial kinetic energy.[18] With review of fully coherent free-electron lasers.[19] Electron accelerator with its associated shielding, generally powered by klystrons, and operated in vacuum with vacuum pumps along beam path. FELs work without a resonant cavity. With X-ray mid-infrared and terahertz FELs, the intense pulses from the X-ray laser lies in the principle of self-amplified spontaneous emission (SASE) where electrons cluster together forming coherent dense waves.

High energy lasers (HEL)

With distances of 1,000 km. x-ray laser beam is inversely proportional to R2 (proportional to I1R2) where R is the distance to a target, we can conclude that RVs are about a factor of 102 (i.e., 1(0) times harder than boosters and that tens of boosters can be destroyed at 1,000 km and tens of RVs can be destroyed at 100 km. With 30 beams, Excalibur can destroy a single booster at about 5,500 km and a single RV at about 550 km.

Laser light scattering involves measuring the changes in number (intensity), the direction (momentum), and the frequency (energy) of each type of photon in the incident and the emerging light beams. Laser related spectroscopy such as multiphoton spectroscopy. As multiphoton absorptions atom or molecule makes a single transition between two of its allowed energy levels by absorbing the energy from more than a single photon, Multiphoton ionization spectroscopy is a sensitive method of recording highly excited energy levels. The sensitivity is enhanced in the technique of resonance ionisation spectroscopy (RIS): two lasers are used such that the frequency of one laser is fixed close to a two-photon allowed transition and the second is tuned to excite a range of higher excited states. Resonance ionization mass spectrometry (RIMS) affords additional species selectivity and sensitivity can is favorable for imaging rare isotope species (diff neutrons) & isotope separation. Two-photon absorption (TPA or 2PA) is the simultaneous absorption of two photons of identical or different frequencies in order to excite a molecule from one state (usually the ground state) to a higher energy, most commonly an excited electronic state. TPA can be measured with are two-photon excited fluorescence (TPEF), z-scan, self-diffraction, or nonlinear transmission (NLT). Two-photon emission (TPE), which is a single electron transition, accompanied by the emission of a photon pair while photon pair conserves transition energy. Moreover, with a 10m diameter 100-MW fibre-optic 1-μm laser array beaming photons on reflector for 58min up to 50,000 km away, laser thermal propulsion (LTP) systems can launch 1,000kg payloads to achieve ΔV of 13.95 km/s with 45-day interplanetary transit time comparable to nuclear thermal rockets (Isp ≈ 3000 s). Laser-based propulsion from Earth orbit can launch spacecraft and payloads with laser thermal propulsion to launch 1,000kg payloads or a 40,000kg payload with 4,000MW Laser to achieve ΔV of 13.95 km/s yielding 2X+ ΔV or departure from Earth.[20]

Theories & equations

$$C = |A||B|sin(\theta) \tag{1}$$

$$F_R = \sqrt{F_1^2 + F_2^2 + 2F_1F_2\cos\alpha} \tag{2}$$

Where, α is angle between $F_1 + F_2, F_R$ is magnitude of resultant vector, based from Euclid's Law of Parallelograms, and Pythagorean theorem. Cross product of parallel vectors is zero and maximum when perpendicular, which suggests lower energy when $\theta_{CME-Laser-Electrons}$ approaches limit θ → 0° and greater likelihood of local electron deposition.

$$\lambda = \frac{h}{mv} = \frac{h}{\sqrt{2.m.K.E}} \tag{3}$$

If 100% of light speed is desired, this suggests a Laser $\lambda_{Electron}$ of 0.002432 nm. Time for laser to contact CME near sun surface of 8.255 minutes. λ_{cme-Fe} and KE values can be quantified from ionisation to elevated charge states based on KE= (Ei-Ef) - K recoil kinetic energy (K) of atom or electron. K.E. and Mass CME values are further outlined in table 1 in Supplementary Information.

$$\Delta E = \frac{hc}{\lambda} = R_\infty \left(\frac{1}{n_f^2} - \frac{1}{n_j^2} \right) \tag{4}$$

Where ΔE is change in energy levels, n_f is final energy level and n_i is initial energy level, R is 1.097E-2 nm⁻¹, which can be used to calculate spectral absorption of photons and electrons. Likelihood of compton scattering & recoiled e- is a time series of free and weakly bound e- in CME that can be calculated based on deBroggle wavelength:

$$\lambda_f - \lambda_i = \Delta\lambda = \frac{h}{mc}(1 - \cos\theta) \tag{5}$$

$$p = \sqrt{E^2 - \left(m_ec^2\right)^2}/c \tag{6}$$

With noticeable shifts in wavelength λ_f of Stellar and refracted photons, Δp, ΔKE, and $\Delta\lambda$ are directly proportional to magnitude, amount of refracted proton/e- flux, and CME split trajectory over dt with noticeable refraction vectors more orthogonal to laser LOS.

The first ionisation energy or minimum joules required to remove an electron from the atom in a gaseous phase

(g) to remove e-, is modeled by He+(g) + e- ⟶ He(g) where Ionisation energy of valence electron in electron volts (eV) of ground state ion is modeled by

$$En = -\frac{Z^2 hcR}{n^2} \tag{7}$$

where Z=atomic number, R is rydberg constant (2.178E-18J) in to excite an electron to higher energy shell. In an external and applied electromagnetic field, aligned electron spin would also yield ($\Sigma J = \Sigma FB \times \Psi$)

$$A_{CME} \approx \left[R\theta_{CME}(R) \right]^2 \tag{8}$$

where CME(R) is the angular width of the plasmoid when the center of the plasmoid sphere is at radial distance R as based from (Moore et al, 2007). CME plasmoid increases in heliocentric angular width, θCME, where frontal cross sectional area, A_{CME}, e CME(R) is the angular width of the plasmoid.

$$PLat = 3nekT = \frac{B^2}{8\pi} \tag{9}$$

Where lateral pressure, p_{Lat}, the final angular width of the CME, Φ_{flare} is flare maximum, n_e is the electron number density, k is the Boltzmann constant, T is the temperature, and B is the magnetic field strength. Final angular width (Final θ_{CME}) in the outer corona and the final angular width (θ_{Flare}) of the flare arcade is $B_{Flare} \approx 1.4$ [(Final θ_{CME})/θ_{Flare}]² based from Moore et al. Moreover, assuming CME area of interest is based on Volume fraction of sphere, rather than CME spheroid ellipsoid equation:

$$\Sigma V_{CME-Cluster} = \iiint 4/3\pi r^2 \tag{10}$$

$$\Sigma \rho_{CME-Cluster} = \frac{Mass}{Volume} \tag{11}$$

$$R_{v,nl} = n_e n_i \sigma_{fb,nl}(v) v \tag{12}$$

R is rate of e- recombinations per unit volume, density of electrons ne, travelling at velocity v, density of positive charges n_i, and the recombination cross section $\sigma_{fb,nl(v)}$. Ionised and polarised CME plasma clouds, reflecting mirror, and e- laser interactions can be modeled by:

$$\Sigma \nabla \circ E = \frac{\rho}{\varepsilon_0} \tag{13}$$

where E is electric field vector divergence gradient, ρ is charge density in coulombs/m^2, ε is dielectric constant of permittivity of free space. In CME's, atoms would be stripped of electrons such as Fe with 3d,4s,3p, 3s shells or energy levels. Total light absorbed is time series.

$$\Sigma v = \frac{\pi e^2}{mc} Nf \tag{14}$$

where e=charge of electron, m is mass of e-, c is speed of light, N is total number of atoms that absorb at frequency V in nm or Hz, f is oscillator strength or ability for each atom to absorb frequency. With measured binding energies (Ev) of Fe, The ground state of Fe is 3d6 4s2 5 D4. Moreover, the EA value of Fe was determined as 1235.93(28) cm−1 or 153.236(34) meV using the slow electron velocity imaging method.[21] Lower energy levels suggests high electron binding affinity for elements with higher FIP such as Fe^{8-16+} and $O^{7/8+}$.

Since CME energy is electromagnetically trapped and can escape as heat, light, or neutral particles,[22] this suggests neutral particles from negatively charged laser or EM field would have P(n) probability % where n is element or particles reaching escape velocity over total particles in CME field of interest.

$$\Sigma P(n) = \frac{Particles\ Escape}{Total\ n\ Particles} x100 \tag{15}$$

Materials and methods

Research investigates design and build of High Energy Laser (HEL) capable of pulsing multi-wavelengths coherent, phase locked X-rays, IR,UV ranging from 10-1 to 10-11λ. Beam wavelengths may be tailored to match helical sin waves of particles oscillating around CME particles and proportional Hz of desired cloud density (age, e-) which holds potential to increase atomic scattering events. Total attenuation is sum of attenuation from photoelectric absorption, rayleigh scattering, and compton scattering. Models simulate recoiled CME e- and domino like compton scattering effect closer to electron beam propagation and plasma cloud charge regions. The origin of pulsed laser would yield greater likelihood of increasing impact and access of pulse from Earth to CME at optimal angles θ>Xdeg rather than head on. Models can analyse directional derivative and eigenvector Hamiltonian dynamics of free scattered e- (Figure 5).
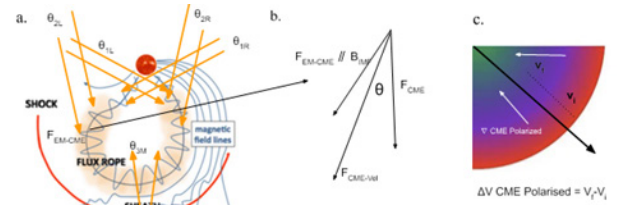

Figure 5 a) $\theta_{1,2,3}$ are angles between laser propagation and CME area of interest, b) Vector and resultant $F_{CME-Vel}$ Vector (V_x, V_y, V_z), c) CME Polarized Gradient, where red is high elevated charge states, purple and green represents neutralised CME particles, formerly elevated charged particles such as Fe_{16+} and O_{7+}/O_{8+}.

Highlighted in Figure 6c, local electron deposition is correlated with reduced velocity or angular momentum. In approaching V_{f-CME} or final velocity of bulk of CME column ionised & polarised particles. If some of front CME plasma orbitals become partially filled by quasi particles, each electron quasi particle separation event would result in more scattering events.
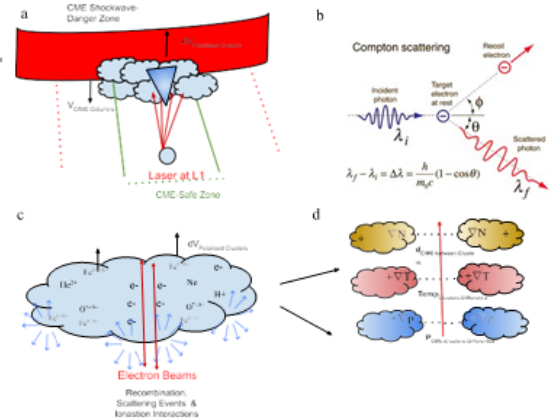

Figure 6 Laser-induced electron recombination and polarization of CME shockwave danger zone with HEL laser at L1/In Orbit. d) Decoupled clusters separated from laser with polar gradient (White=Neutral, Yellow = +).

If the electrons have low velocity components relative to the moving plasma, recombination and ionisation would be accelerated. Photo Ionization and recombination rates can also be expressed in Milne relations toward accurate predictions. Electron gas approaches 0 charge state as thermal processes (photons or electron collisions) compete with ionization rates. For recombinations to the ground state, the photon released can also ionise other atoms. For dense plasma, sum of electron recombinations in local cluster to all levels except for the ground state model effective recombination coefficient, or "case B" recombination. In approaching $\Delta\rho$ and ΔE with decrease in charge density in coulombs/m^2 and E-Field near electron beams, $\Delta\rho$ lim $\rightarrow$ n suggests greater probability of decoupling FIP elements and layers and correlated ∇V or d $<Vx,Vy,Vz>$ to identify optimal neutralisation time intervals, charge, temperature and pressures between clusters.

As gradient distribution and density of coronal e- in CME are also correlated to $t_{Cluster-Separation-n}$ or-time to cluster separation of CME $Cluster_n$ and $d_{CME-Clusters}$ cluster separation distance range, accelerated separation, neutralisation, and higher e- recombination events to ground state may suggest higher local density of coronal e- freed in CME. In approaching robust CME data observations and data transmission with near-real time characterisation of CME, Other laser LPP propagation strategies may include identifying and freeing coronal e- inside CME cluster layers (Figure 7).
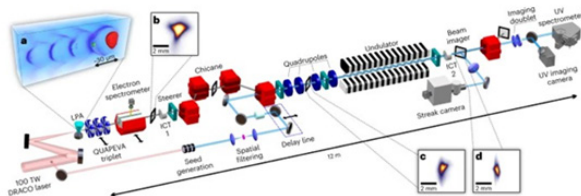

Figure 7 Seeded free-electron laser driven by a compact laser plasma accelerator. (Labat, et al, 2022).

Design and build of high energy lasers

A compact laser plasma accelerator can be reduced in size from 100m+ to <1m. A Plasma lens can control over the radiation wavelength reduce divergence of electron clusters and external laser-light pulses into the undulator can accelerate and improve beam quality. High-energy-density electron beam is generated with laser peak intensity of 4×10^{23} W cm^{-2}, a maximum density of 117-180nc and a kinetic energy density up to 8.79×10^{18} J m^{-3} with 416 MeV temperature beam and beam divergence of 7.25°C. As the laser peak intensity increases (e. g., 10^{24} W cm^{-2}), both the beam energy density (3.56×10^{19} J m^{-3}) and the temperature (545 MeV) are increased, and the beam collimation is well controlled. With Electromagnetic alignment from undulator, electrons or photons change spins and angular momentum. With 1370 watts per square metre (W/m2) in uG around 1AU, 1000 metre solar panels could power a MW HEL laser with 1760 kg solar panels with 1.76 kg/m² for 3 mil thickness coverglass. Since IR and radio waves penetrate through Earth's atmosphere a laser beam on Earth's surface coupled with IR/radio waves may induce scattering and reduce systems mass.

Laser subsystems may include beam splitter, chirped pulse amplification, viscoelastic dampers, and low absorption counterparts. Phase locked, multiwave stacked field holds potential to deliver more waves or energy in laser beam. With a two-port e- beam splitter to achieve maximal electron transfer, recombination and CME scattering area, efficient two-port beam-splitting can be accomplished from a half-silvered mirror, a waveguide coupler, or a fiber switch. With the intensity in diffracted beams blocked by an aperture, quantum

interaction-free measurement (IFM) design combines an electron resonator with a weak phase grating with scattering matrix to analyse performance of beam splitter.[23] As electrons are passed through weak phase grating multiple times within the resonator, the beam-splitting ratio is controlled by the number of passes through the grating Fast switching gates allow electrons to enter and exit the resonator and scattering matrix method can analyze the performance of the beam splitter based on.[23] A laser with chirped pulse amplification (CPA) may yield high NICS scattering, whereby NICS photons can be indirectly observed from energy shift in e- output and positron generation.[24] Replacing all intracavity optics and coatings with low absorption counterparts (4x), increasing the number of degrees of freedom of the correction system (1.3x), homogenising the pump irradiance profile (net 2x) and compensating for depolarizing effects (>4x) (LaFortune, SPIE Photonics). Moreover, viscoelastic dampers (VEDs) to reduce micro vibration suppression of space truss structures and significantly improve the pointing stability of the optic camera (Figure 8).
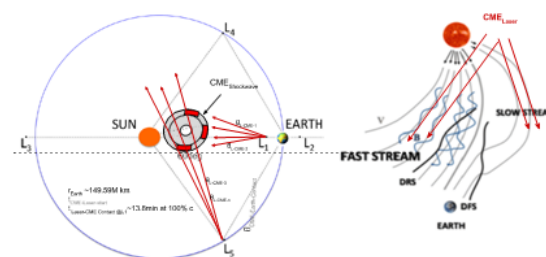

Figure 8 a) Orbital geometry of CME from L1, L5, L4; and b) CME laser on CME slow vs fast stream.

Results and discussion

Orbital geometry and locations of space-based laser for CMEs

If laser is based at L1 1.5M km from Earth, this provides direct 100% Line of Sight (LOS) to CME ions along trajectory that impact Earth compared to L4/L5, which would require laser to beam through a CME Arc Length$_{.5AU}$ of ~29.06M km of ionised atoms, if .5AU is limit and laser-CME Zone LOS cut off frequency or access window (Figure 9).
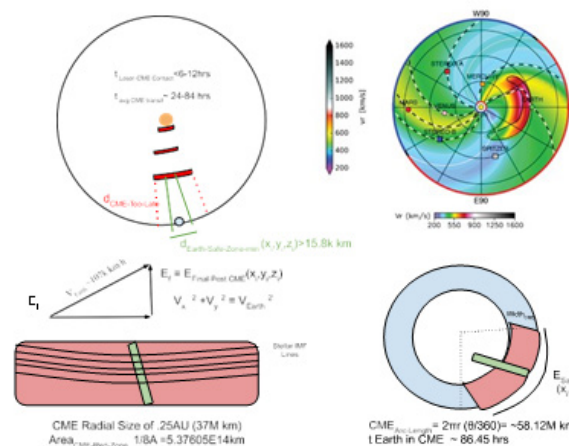

Figure 9 CME area, linear geometry, and time to impact analysis.

Linear Models are based on CME shockwave instead of slow/fast stream of particles that oscillate radially outward. With 800-100km/sec of ionised particles in Figure 8b, highlighted in red, data suggests

higher velocity is correlated with higher particle density of ionised particles with elevated charge states such as Fe16+. Width and height of CME radial size are based on 800-1000 km/sec shockwave, which is CME Shockwave Zone.

Average CME radial size is 0.25 astronomical unit (AU; 37M km,) when passing Earth at 1 AU (150 million km). CME Velocity of 2,160,000km/hr is 20X greater velocity than Earth orbital speed (V_{Earth}) of 67,000 mph (107,000 km/h) around the star. For Earth to travel <9.2M km path through CME suggests 86.44 hrs (3.6days) time window through CME, which provides baseline estimate for laser to clear path. Where $Width_{CME}$ is approximate distance ($d_{Earth-Travel-through-CME}$) and $d_{Laser-CME-Free-Path,}$ minimum Earth safe zone gap is $d_{Earth-Safe-Zone-min}$ (x_i,y_i,z_i)>15,800 km around Earth's Radius and MEO and 43,164 km around GEO.

With laser Velocity (km/hr) at 100% light speed, laser beam contacts CME <8.2557 minutes from L1 to CME near Sun surface, excluding light alignment with mirrors. As some CMEs accelerate between ~0.1 and ~0.2 au, further research may explain how some CMEs accelerate from 500-800 km/sec with dV of 300km/sec. Early contact prior to acceleration further suggests CME ions may have higher charge states and ionisation FIP rates. After 8.2557 minutes, CME travelling at 600km/sec would be 297,206km (.00198AU) away from star with area of CME Shockwave Zone Area (1/8A) of 192,709,234 km2. If heliocentric angle (ψ) is <2° after 8.2557 minutes, this suggests CME Arc Length of 10,374 km, consistent with (Moore and Sterling, 2007). At 297,206 km radial distance, angular widths of 20-40° correspond to CME Arc lengths of 103,744-207,489km, respectively. At 1AU with (ψ) ~40°, CME Arc Length is around 104,440,502km without contact from laser or electrons.

Outlined in Table 1 early laser-CME contact suggests Length Ratio w/o Reflectors of 1 $CME_{t=8.255}$: 10,067km $CME_{t=1AU}$, or for every 1 km gap laser creates at t=8.255min at .00198AU creates a 10,067 km gap for Earth to orbit through. In Table 2, $d_{Earth-Safe-Zone-min}$ and $v_{Earth-Safe-Zone}$ is distance or diameter of planet and volume around planet

to orbit through CME. As arc length at leading edge of $CME_{Initial}$ at t=8.255min, CME Clearance Arc Length of 4.29km is suggested to achieve $d_{Earth-Safe-Zone-min}$ of 43,164km gap around GEO Table 3.

Table 1 CME after contact with electrons km²

CME Parameters after Contact with Laser, Electrons, Reflectors		
CME distance at Edge (at t=8.255min)	297,206	km
CME distance	0.00198	AU
Heliocentric angle	2	degrees
CME Area (1/4A)	385,418,469	km²
CME Shockwave Zone Area (1/8A)	192,709,234	km²
CME Arc Length (initial w/out reflector)	10,374	km
CME Arc Length (w/ Reflector @ .387AU)	30,316,369	km
CME Arc Length (final at 1AU)	104,440,502	km
CME Length Ratio w/ Reflectors	3	km
CME Length Ratio w/o Reflectors	10,067	km

Table 2 CME separation requirements from neutralisation at t=8.255min

CME Separation Req from Neutralisation/ Electrons at t=8.255 min	
Laser Velocity @ 100% Light Speed	299M
dEarth-Safe-Zone-min (xi,yi,zi)	15800
dEarth-Safe-Zone (xi,yi.zi)	31600
dEarth-Safe-Zone-GEO (xi,yi,zi)	43164
Volume Earth Safe Zone min Km3	1.65219E+13
Volume Earth Safe Zone GEO Km3	3.36863E+14
Min CME Clearance Arc Length	1.57
CME Clearance Arc Length	3.14
CME Arc Length around GEO	4.29
CME Radius Equivalent Laser Clear GEO	123
CME Area Equivalent - Neutralisation Zone	47399
CME Volume Equivalent - Neutralisation Zone	7762789

Table 3 Neutralisation volume & laser pulse rates, for CME Safe Zone of 4.29km around Earth/GEO

Laser-CME-Contact Time (min)	CME Neutralisation Arc Gap Rate(km/min)	CME Neutralisation Area (km²/ min)	CME Neutralisation Volume (km³/min)
10	0.0429	4740	776.279
30	0.143	1580	258.76
60	0.071	790	129.38
120	0.036	395	64.69
180	0.024	263	43.127
240	0.018	197	32.345
300	0.014	158	25.876

CME Area Equivalent - Laser of 47,399 km^2 and CME Volume Equivalent of 7,762,789 km^3 corresponds to 2D area and 3D spherical volume of ionised particles and columns to neutralise to achieve 4.29km Arc Length $d_{Earth-Safe-Zone}$ at 1AU. With laser scan swath width from right to left or to move CME particles in plane behind Earth trajectory, CME Neutralisation Arc Gap Rate (km/min) corresponds to laser rotational pulse sensitivity requirements without mirrors. If Laser-CME Contact Time of 60 minutes is achievable, this suggests 60 minutes to neutralise CME plasma clouds for each .036 km along CME shockwave edge or column and Neutralisation Area of 789.98 (km^2/min). With 60min Laser CME contact time, average 129,380 km^3/min of CME would need to be partially to full neutralised or separated by sufficient CME ion distance.

There are also several neutralisation strategies such as $\theta_{Laser-CME}$, swath rate, and laser pattern, which e laser geometry or signature imprinted on CME edge. Laser Pulse Parameters (LPP) or Neutralisation gradient patterns (NGPCME-Laser) for analysis include Spiral (centre radially outwards), S pattern, zig zag, etc. LPP or NGPCME-Laser defines laser swath Scan Rate, Swath Width, Scan Direction, etc that may be correlated with CME electron pairing and ion scattering events.

With beam geometry of a cylinder, e- density in beam is correlated with change in electric field beam strength intensity, which could be measured as flux at mirrors and correlated with electron transfer rate in CME cluster.

If assuming a 10-50% e- transfer rate linear and Fe is clustered at various angles to electron recombination angle, density gradient forms of Fe or CME atoms after recombination with rapid deposition of electrons to fill valence shells from Fe^{16-20+} to Fe^{4-2+}. Models and experiments may quantify optimal electron wave density and e-transfer rate based on local charge states.

Assumptions in current models may include constant radial acceleration growth and uniform ionised atom column density, laser split at 50% middle of CME Shockwave, and not factoring in growth, scattering events, etc. More research will also quantify potential savings of mitigating CME around Earth LEO vs GEO. If 4.29km gap around GEO with contact to $CME_{t= 8.255min}$ is achievable, future research will quantify time for electron neutralisation requirement contact time, scattering, FIP, and e- recombination rates (Figure 10).
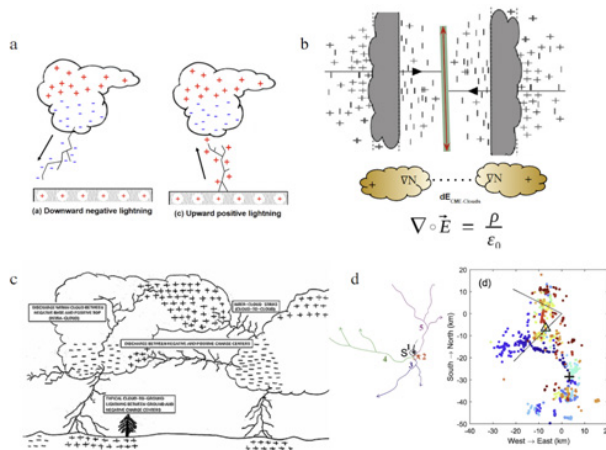
Figure 10 a) - and + lightning from clouds on Earth, b) Laser contacting CME cloud creating EM field charge gradient, c) Intracloud lightning between opp charge regions w/o return stroke but slower recoil Streamers (NASA GHRC, 2023) d) Channels of + leader & lightning activities with + stroke and - strokes (△) (jiang, 2021).

Lightning, CME plasma, cloud charge dynamics and laser interactions

Clouds on Earth have excess + charge near cloud tops, and - charge in bottom layers, bounded by charge clusters in each layer. Inverted charge distribution has - layer of electrons on bottom. As the EM field around clouds become stronger, positive ions and free electrons are stripped to form lightning. Similar to how lightning bolts of electrons induce the temperature of the surrounding air and pressure to rise, electron laser beam generates sharp temperature, pressure, and electromagnetic gradients, outlined in Figure 7d and 8b. Pressure in this region may become incredibly high, resulting in sonic shock waves of particles in most directions. Once CME ions interact with electron laser beam, dart and recoil lead (RL) branches may form. Lightning dart and recoil branches or leaders are current pulses that propagate along lightning channels, reionising the channel. As observed in clouds on Earth, previously ionized channels can undergo dielectric breakdown multiple times at intensities with most recoil activity at very inner region of the corona sheath. Outlined in Figure 8d), observations of a special intracloud (IC) lightning flash from involving multiple positive leader branches after measuring relative luminosity variation (blue curve), the fast electric field, radiation, and magnetic field changes in lightning clouds.[25] Connection of recoil leaders (RL) with intracloud (IC) lightning helps to create bipolar upward flashes and their interaction with IC flashes.[26] While the most common IC pulses are small amplitude and narrow IHC width, pulses temporarily matched optical emission are often larger amplitude

such as >1V/m with larger pulse width around >20us. Vertical extent of IC also had greater VLF source frequency and optical emission.[27]

If negative e- are scattered closer to beam edges of CME ion clusters and various layers, this would form a repulsive electrical field gradient that could electromagnetically alter, attract, and/or bound cloud layers. As CME Plasma cloud also does not propagate through a vertical electric field, - charge recoils or Branches may propagate at $\theta_{Recoils-n}$ more toward + clusters such as Fe16+ regions or rows. Some recoils and branches may or may not be advantageous for CME cloud divergence gradient, characterised by net movement from local electron light beam (Figure 11).
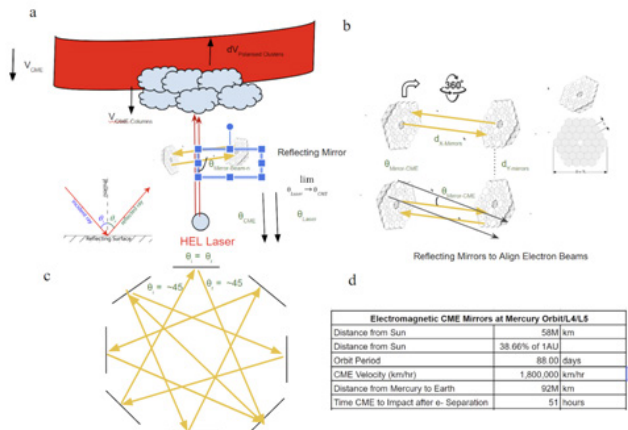
Figure 11 a) Cartoon of laser, mirror, CME interactions, vectors, angles, b) Reflecting mirrors to align laser more parallel to CME cluster velocity, <V_x,V_y, V_z>, c) 360° mirror network similar to Dysons sphere.

Reflector mirrors to align laser and neutralise ionised particles

Polarisation or altering the trajectory of high energy particles with elevated charge states demands active systems such as a reflecting mirrors or fence, similar to dyson's sphere. If maximum electron deposition occurs when Laser beam and CME resultant vector velocity are parallel, this suggests laser waves tangent or derivative of CME particle velocity <Vx, Vy, Vz) would have corresponding electron absorption and recombination rates per θCME-Electron-Laser degree. If higher rates of valence electron pairs are filled when $\theta_{laser} \approx \sim\theta_{CME}$, this suggests EMC electromagnetic compatibility-electron waves combine in phase, angular momentum spin vectors add up to high irradiance and combined effect with waves of larger amplitude. Considering velocity of CME is greater than laser speed of light, this also suggests optimal mirror alignment ranges to laser and CME whereby θi<5-10° and ~θCME<5-10°.Mirrors and beam may be angled for scattering and absorption events to pull CME clusters behind Earth trajectory.

If e- light distribution that is more spread out yields higher FIP ionisation rates, this suggests less dense beam distribution. Subsystems integrated into mirrors include imaging sensors, beam light scatterer, semiconductor or insulator, and to deflect e- based on inverse free electron laser (IFEL), ICS compton scattering for electron beam pointing control based on.[28,29] Semiconductor Si plate generates plasma to modulate e- density gradient.[30] Deflection of pulses and accelerated electrons in a laser-plasma accelerator (LPA) are controlled via laser pulse front tilt and transverse density gradients for e- steering.[28] Reflecting mirrors could reflect light from laser at up to 1c 100% light speed along Earth-CME trajectory after CME Shockwave and Ions, to continuously separate CME plasma clouds throughout majority of CME transit to planet.

Citation: Lutz K, Trevino T. High energy laser & systems to neutralise stellar coronal mass ejections (CME) plasma. *Aeron Aero Open Access J.* 2024;8(1):1–9.
DOI: 10.15406/aaoaj.2024.08.00187

Following signal transmission of impending CME, mirrors move into position to reflect. Mirror network may grow to encompass primary and secondary mirror pairs that are separated by optimal distance dY-mirrors to allow for HEL laser electron coupling. If > dMirrors distance between mirrors suggests more time and higher rates of electron shells are filled, this suggests mirrors maintain higher coherent electron paths after light reflection between mirrors for multi km to hundreds of km dMirrors distances. Mirrors may have materials and systems similar to James Webb space Telescope (JWST) with Ag secondary convex mirror .74m diameter, moved by AOS six actuators.

Algorithms may align each mirror segment to less than half a micron or so to ensure a majority of light is maintained within mirror network. Further R&D will evaluate how to position mirrors for optimal e- absorption and scattering events. If higher CME plasma cloud cluster separation is achievable closer to CME propagation, the mirror network, $d_{Mirrors}$ distance, systems, and upmass could be minimised and conserved. This suggests reflecting mirrors in closer orbits to local star. If Mercury Lagrant points such as L4/L5 may provide greater LOS to CME path, Mirror network positioned closer to local star around 58-70 million km from 38.66% distance to 1AU would provide <92M km or time till CME would impact Earth. To maintain thermal equilibrium in closer orbit with temperatures of 500 degrees Celsius (590-725K) on sun side, CME Mirrors may have heat shield or stellar panels to absorb and even transmit energy from solar radiation and CME. If a heat shield provides thermal equilibrium instead of energy collection, hot side may be coated with silicon, vapor deposited aluminum (VDA), and Kapton E- substrate coatings, similar to JWST. Moreover, considering large million kilometre distances of CME, other systems such as electromagnetic pulse (μg-EMPs). Similar to how negative electron air ionisers add electrons to air molecules, uG EMPs add e- to particles in vacuum and may be activated by data transmission, laser or CME contact.

Moreover, if Laser Velocity is pulsed at 100% speed of light (c) this suggests, CME-Laser Velocity Ratio of 0.20% and Laser-CME Velocity Ratio of 500, which suggests electron beam is 500X faster than CME Ionised particle 600 km/sec velocity. Further research may evaluate coherent electron beam to customise and match CME element composition, density, behaviour, and frequency.

Further research and ground experiments

Future research discusses several factors contributing to CME trajectory including: (i) CME Cloud Density, Trajectory , (ii) CME Atomic composition & Polarity, (ii) HEL Laser on Coronal EM fields lines, (iii) HEL Laser Direct Contact Effects, (iv) HEL Laser InDirect Post-Contact Effects. Ground experiments may simulate and measure CME plasma cloud conditions, density, distribution, recoils, and interactions of Ionised gas particles of Fe +16, O7+/8+, He2+, Ne, etc. And electron laser interactions at various contacts and reflecting mirror angles. Charge-state selective recombination rate coefficients can be measure charged ions via TOF electron-beam ion trap based on (Lindroth, et al) With an analyzer, detector arrays, multiphoton spectroscopy, and multiple electron beam sources, free electron laser based on.[18] For data recording and analysis, algorithms for static laser light scattering calculates exact particle size distributions even for (semi-)transparent, opaque, round, and non-round particles. Experiments measure CME plasma cloud-laser recoil branch interactions via radio VHF (30–80 MHz) with TRI-D interferometric imaging algorithm based on (hare, et al). White-light coronagraph data provides comprehensive central position angle, the angular width and heliocentric distance of 7,000 observed CME's between 1996-2002.[31] Telescopes can image White-light coronagraphs telescope,

which also are produced via Thomson scattering of sunlight off of free e- within the CME plasma.

Models may factor in and quantify plasma-laser- electron neutralisation requirement contact time, scattering events, e-recombination rates, and CFD and MHD algorithms. If slower pulsed HEL velocities would yield increased electromagnetic attraction with CME plasma species, this may better attract or separate CME plasma ions. If telescopes can image CME and transmit data to HEL in near real time, the laser may even customise and match CME element composition, behaviour, and frequency. If in-space mirrors could reflect and/or absorb some of HEL beam energy, this may suggest a reflector network could reduce laser or e- distribution, intensity and velocity.

Conclusion

As CME's can lead to outages in telecoms, GPS systems and collapse of electric power grids, multipurpose high energy lasers (HEL) approach holds potential to mitigate CME carrington flares, enable beam laser propulsion (BLP), and support planetary defense. If approaching $\theta_{Laser} \approx \theta_{CME} \approx \theta_{Mirrors}$ yields greater electron-CME recombination rates, this suggests mirror architecture is advantageous and greater rates of Electromagnetic Compatibility (EMC) and valence e- pair fill rates/degree to neutralise elevated charge state ions such as Fe16+.With higher ambient plasma density, early contact prior to acceleration suggests CME ions may have higher charge states and ionisation FIP rates. A space-based laser and mirrors may even polarise elements at ly distances across Interstellar Medium (ISM) and during star and planet formation.

Author contributions

The authors are the primary contributor to this work and are responsible for this study. The authors confirm this material or similar material has not been submitted to or published in any other publication. Copyright © 2024 by Kole Lutz. Published by the Aeronautics and Aerospace Open Access Journal (AAOAJ), with permission.

Author disclosure statements

References

1. Kay C, Airapetian VS, Lüftinger T, et al. Frequency of coronal mass ejection impacts with early terrestrial planets and exoplanets around active solar-like stars. *The Astrophysical Journal*. 2019;886(2).

2. Lepping RP, Jones A, Burlaga LF. Magnetic field structure of interplanetary magnetic clouds at 1 AU. *Journal of geophysical research*. 1990;95: 11957–11965.

3. Moore RL, Sterling AC, Suess ST. The width of a solar coronal mass ejection and the source of the driving magnetic explosion: a test of the standard Scenario for CME Production. *The Astrophysical Journal*. 2007;668(2):1221–1231.

4. Nitta NV, Mulligan T, Kilpua EKJ. et al. Understanding the Origins of Problem Geomagnetic Storms Associated with "Stealth" Coronal Mass Ejections. *Space Sci Rev*. 2021;217(82).

5. Geiss J, Gloeckler G, Von Steiger R, et al. The southern   high-speed stream: results from   the SWICS instrument on Ulysses. *Science*. 1995; 268:1033–1036.

6. Lepri ST, Laming JM, Rakowski CE, et al. Spatially dependent heating and ionization in an ICME observed by both ACE and Ulysses. The Astrophysical Journal. 2012;760(2).

7. Gu C, Meisner VH, Schweingruber RF, et al. Detailed composition of iron ions in interplanetary coronal mass ejections based on a multipopulation approach. *Astronomy and Astrophysics*. 2023;671.

8. Landi E, Alexander RL, Gruesbeck JR, et al. Carbon ionization stages as a diagnostic of the solar wind. *The Astrophysical Journal*. 2012;744(100).

9. Dere KP, Landi E, Mason HE, et al. CHIANTI - an atomic database for emission lines. *Astronomy and Astrophysics Supplement Series*. 1997;125:149–173.

10. Rakowski CE, Laming JM, Lepri ST. Ion charge states in halo coronal mass ejections: what can we learn about the explosion? *The Astrophysical Journal*. 2007;667(1):602–609.

11. Dalla S, Marsh M, Zelina P, et al. Time dependence of Fe/O ratio within a 3D solar energetic particle propagation model including drift. *Astronomy & Astrophysics*. 598.

12. Zurbuchen TH, Weberg M, Steiger RV, et al. Composition of coronal mass ejections. *The Astrophysical Journal*. 2016;826(1).

13. Alvarado-Gomez. Suppression of coronal mass ejections in active stars by an overlying large-scale magnetic field: a numerical study. *The Astrophysical Journal*. 2018;862(2).

14. Bemporad A, Pagano P, Giordano set al. Measuring the electron temperatures of coronal mass ejections with future space-based multi-channel coronagraphs: A numerical test. *Astronomy & Astrophysics*. 2018;619.

15. Li X, Wang Y, Liu R, et al. Geophys. *J Res Space Phys*. 125.

16. Vrsnak Bojan, Vrbanec Dijana, Čalogović Jasa, et al. The role of aerodynamic drag in dynamics of coronal mass ejections. *Proceedings of the International Astronomical Union*. 2008;4:271–277.

17. Kim T, Moon Y, Na H, et al. Comparison of CME radial velocities from a flux rope model and an ice cream cone model. *The Astrophysical Journal*. 2011;839:2.

18. Fisher A, Park Y, Lenz M, et al. Single-pass high-efficiency terahertz free-electron laser. *Nat Photon*. 2022;16:441–447.

19. Feng C, Deng HX. Review of fully coherent free-electron lasers. *NUCL SCI TECH*. 2018;29:160.

20. Duplay Emmanuel, Bao Zhuo, Rosero Sebastian, et al. Design of a rapid transit to Mars mission using laser-thermal propulsion. *Acta Astronaut*. 2022;192:143–156.

21. Chen X, Luo Z, Li J, et al. Accurate electron affinity of iron and fine structures of negative iron ions. *Sci Rep*. 2016;6:24996.

22. Reames Donald. Fifty Years of 3He-rich Events. *Front Astron Space Sci*. 2021;27.

23. Yang Y, Kim CS, Hobbs RG, et al. Efficient two-port electron beam splitter via a quantum interaction-free measurement. *Physical Review A*. 2018;98(4).

24. Bamber C. Studies of nonlinear QED in collisions of 46.6 GeV electrons with intense laser pulses. *Physical Review D*. 1999;60:92004.

25. Jiang R, Yuan S, Qie X, et al. Activation of abundant recoil leaders and their promotion effect on the negative-end breakdown in an intracloud lightning flash. *Geophysical Research Letters*. 2022;491.

26. Cruz IT. Upward bipolar lightning flashes originated from the connection of recoil leaders with intracloud lightning. *Geophysical Research Letters*. 2022;49:22.

27. Brunner KN. Explorations in intracloud lightning and leader processes. *Theory of Computing Systems, Math Systems Theory*. 2016;57.

28. Mittelberger. Laser and electron deflection from transverse asymmetries in laser-plasma accelerators. *Physical Review E*. 2019;100.

29. Gadjev I, Sudar N, Babzien M, et al. An inverse free electron laser acceleration-driven Compton scattering X-ray source. *Sci Rep*. 2019;9:532.

30. Sakai. Electron-beam–controlled deflection of near-infrared laser in semiconductor plasma. *J Appl Phys*. 2023;133(14):143102.

31. Yashiro. A catalog of white light coronal mass ejections observed by the SOHO spacecraft. *Journal of Geophysical Research (Space Physics)*. 2004;109:7105.